# Dissolution of silica component of glass network at early stage of corrosion in initially silica saturated solution

Dien Ngo[1], Hongshen Liu[1], Huseyin Kaya[2], Zhe Chen[1], and Seong H. Kim[1,2*]

1. Department of Chemical Engineering and Materials Research Institute, The Pennsylvania State University, University Park, PA 16802, USA.

2. Department of Materials Science and Engineering, The Pennsylvania State University, University Park, 16802, USA.

*Corresponding author: shkim@engr.psu.edu

## Abstract

Corrosion of glass in silica-saturated solution has been performed with the assumption that dissolution of silicate species from the glass network would not occur. Using surface-sensitive analytical techniques, we report experimental evidence suggesting the dissolution of silicate network species from a model nuclear waste glass, called international simple glass (ISG), in an aqueous solution initially saturated with soluble silica species. Results from low energy ion scattering and x-ray photoelectron spectroscopy reveal a complete depletion of mobile element species (B, Na) from the ISG surface and an enrichment of Zr on the outmost surface. In support of spectroscopic analyses, results from topographic imaging with atomic force microscopy show a stochastic dissolution of glass surface resulting in a higher surface roughness with increasing corrosion time in aqueous solution. This study shows that a true equilibrium between soluble silica species in the solution phase and silicate species in the glass network could not be warranted by performing corrosion experiments in the solution where dissolved silica species are initially equilibrated with amorphous silica in the presence of KOH. The leaching of mobile species (B,

Na) could affect the saturation level of aqueous solution and induce further dissolution of the glass surface.

## 1. Introduction

Aqueous corrosion of glasses used for immobilization of nuclear waste materials has been extensively studied in recent years.(1-4) The glass corrosion process generally evolves through three stages.(5, 6) The stage-I is associated with a fast corrosion rate in dilute solution conditions, which leads to the formation of a so-called alteration layer. As the alteration layer grows thicker and the solution concentrations of soluble species leached from the glass approach the saturation, the corrosion rate decreases to an extremely low state. The steady state with the extremely slow dissolution rate is called stage-II; in this period, the surface film protects the glass from further corrosion by limiting the transport of mobile species through the layer.(5, 7) Sometimes, after a long time in this latency period, the fast corrosion process resumes; this is called stage-III.(8) Understanding the corrosion mechanism of glass and the stability of the alteration layer in stage-II is important to predict the durability of glass used for nuclear waste immobilization.(1, 9-11)

The glass corrosion process is extremely complicated because it involves chemical reactions of a non-equilibrium material (glass) in a non-equilibrium condition (extremely slow kinetics). Due to this nature, the reaction products (for example, the composition and structure of alteration layer) can vary depending on the glass composition and surface preparation history.(11-13) In addition, the initial condition of the aqueous solution can also affect the glass corrosion behavior.(10, 14-16) Moreover, the effects of initial surface conditions on glass corrosion have not been studied extensively.(11, 13) So, it is very important to properly prepare and fully characterize

the glass surface and precisely control the corrosion condition for a better understanding of corrosion mechanisms.

Based on the thermodynamic affinity model,(17, 18) if the glass is immersed in the initially silica-saturated solution, then the dissolution of silicate network components from the glass would not occur or at least be negligible.(9, 19, 20) In this condition, the corrosion is thought to be dominated by the transport of water molecules and leachable ions (mostly alkali modifier ions and boron network formers) through the gel layer being formed between the solution and pristine bulk glass phases.(7, 9) Among the network formers, Si is the most abundant in typical silicate glasses and expected to be stable because the initial solution is saturated with the soluble silica species. Other network formers are B, Al and Zr. The B species is easily dissolved.(1, 7) The Al species is believed to be stable as long as the solution pH is higher than 4.(1, 10, 20, 21) The Zr species is considered to be practically insoluble because the solubility product constant ($K_{sp}$) of its hydroxide is extremely small.(22) Based on this model (or assumption), the depth profiles of various elements measured with time-of-flight secondary ion mass spectrometry (ToF-SIMS) are often normalized with the Zr signal.(1, 20, 23)

In this study, we tested if this thermodynamic affinity model is valid at the inception of the stage-II corrosion by analyzing the surface composition and topography of a model nuclear waste glass after treatment with the silica-saturated solution for short periods of time (from 100 seconds to 7 days). International simple glass (ISG) was chosen for this study.(3) Its composition is given in Table 1. To minimize the variance in surface conditions and prepare the surface closest to the bulk composition, fractured surfaces were used. The composition of the outermost layer of the fractured surface was analyzed using low energy ion scattering (LEIS).(24) Changes in surface composition after corrosion in the silica-saturated solution were monitored using LEIS and x-ray

photoelectron spectroscopy (XPS). The topography of the corroded surface was characterized by atomic force microscopy (AFM). The results from these analyses suggest that the thermodynamic affinity model may not be valid for the ISG glass in the pre-silica-saturated solution at least at the beginning of stage-II corrosion.

## 2. Experimental Details

### 2.1. Sample Preparation

The ISG used in this study was provided by MO-SCI Corporation. Small discs were cut from the received bar and then cleaned thoroughly by sonicating with ethanol and acetone. The freshly fractured surface was used for corrosion treatments. In this way, any structural and compositional defects resulted from sample surface preparations such as mechanical polishing or cleaning could be avoided. The aqueous corrosion solution saturated with soluble silica species at 90 $^{o}$C was prepared following the protocol described in Ref. (1). The amorphous silica was added to ultrapure water in a 500 mL PFA jar (Savillex Corporation) and 0.5 M KOH solution was used to increase the pH of silica containing water to 10. This pH adjustment was performed to accelerate the dissolution of amorphous silica in water. After holding the jar in an oven at 90 $^{o}$C for a week, the pH of the solution was adjusted to 7 and this solution contains 5.09 mM of soluble silicon containing species and ~ 0.1 mM of $K^{+}$ ions.(1) When the solution temperature is dropped to room temperature, then the dissolved silica concentration decreases to 1.91 mM.(25) The ISG glass sample (0.5 cm x 0.5 x 0.5 cm) was kept on a PFA mesh support screen (Savillex Corporation) immersed in a 350 mL leaching solution in the 500 mL PFA jar. The corrosion experiments were done in an oven held at 90 $^{o}$C. The pH of corrosion solution was kept at 7.0 ± 0.5 using 0.5 M HCl and 0.5 M KOH solutions. The ratio of sample surface to solution volume (S/V) was kept low (~

0.43 $m^{-1}$) to avoid significant changes in solution composition due to glass corrosion. The corrosion time was varied from 100 seconds to 1 hour, 1 day, and 7 days. After taking out of the solutions, the samples (except the 100 s treatment) were rinsed thoroughly with ultrapure water (18 MΩ·cm resistivity) and then dried using a dry nitrogen blow. They were then immediately mounted to the LEIS chamber. After LEIS analysis, the same samples were analyzed with XPS and AFM.

**2.2 Compositional analysis of topmost surface with low energy ion scattering (LEIS)**

Changes in elemental composition of the top atomic layer of pristine fractured surface and corroded surfaces were determined using a Qtac100 LEIS instrument (ION-TOF, Chestnut Ridge, NY).(26) The spectrometer was equipped with a double-toroidal Calipso energy analyzer. The primary ion source was a 3 keV $^4He^+$ beam at the surface normal incident angle. This primary ion source condition was chosen to maximize the sensitivity of a broad range of atomic masses (from 16 amu of oxygen up to 91.22 amu of zirconium). The atomic mass of boron (10.8 amu) is too small to be detected in this condition. The scanned area was 1000 × 1000 $\mu m^2$ with a typical ion dose of 2 x $10^{14}$ ions / $cm^2$. The $^4He^+$ ions scattered from sample were collected at an angle of 145°. During LEIS measurements, an electron flood gun was used for charge compensation on the sample surface. All spectroscopic experiments were done at room temperature in a vacuum chamber of ~$10^{-9}$ mbar. To study the composition of clean pristine ISG surface, a sample was fractured under ultrahigh vacuum before being transferred to the spectrometer. In LEIS analyses of the corroded ISG samples, sample surfaces were first cleaned by sputtering with a 0.5 keV $Ar^+$ beam before being probed by the primary ion beam. The LEIS spectra were fitted using the CASA software package with a Shirley baseline. The peak area of each element obtained from the fitting was normalized by the peak area of oxygen.

The extreme surface sensitivity of LEIS comes from the fact that a low energy ion beam is used and only ions scatter off from the outermost layer are detected.(27, 28) The low energy does not allow ions to penetrate too deep into the surface and they mostly collide with atoms on the outermost surface. Due to the lack of matrix effect in LEIS analysis the LEIS signal is proportional to the surface concentration of elements.(27, 28)

**2.3. X-ray photoelectron spectroscopy (XPS) analysis of ISG surfaces**

XPS analyses of ISG surfaces were carried out with a PHI VersaProbe II system equipped with a monochromatic Al-Kα x-ray source.(29) The probe depth was about 10 nm and the spot size information is ~ 4 $mm^2$. The low-resolution scans were performed for O 1s, Na KLL, Ca 2p, B 1s, Zr 3d, C 1s, Si 2p and Al 2p regions at a pass energy of 117 eV. The high-resolution C 1s spectra were collected with a pass energy of 29 eV.(29) Peak fitting is performed for C 1s spectra by a Voigt function (65% Gaussian, 35% Lorentzian) for adventitious carbon correction. Details of relative sensitivity factors (RSFs) determination of all elements of ISG and spectra processing and quantification were described in previous work.(11) The concentration for each element was obtained by averaging the results of three random spots.

XPS depth profiles for element of Na, B, Al, Ca, and Zr on corroded ISG were performed by the same XPS instrument. An $Ar^+$ beam with an energy of 4 kV was employed for the measurement. The sputter rate was determined by performing depth profiling for $SiO_2$ film with a known thickness. The corresponding scanning steps for samples corroded for 1 h, 1 d, 7 d are 80 nm, 80 nm, 120 nm, respectively. The crater depth created during XPS depth profile measurements was 400 nm, 800 nm, and 3200 nm for 1 hour, 1 day, and 7 day-corroded samples, respectively.

**2.4. Topography analysis with atomic force microscopy (AFM)**

The surface topography of uncorroded and corroded surfaces of air-fractured ISG samples was characterized using AFM (Nanoscope V Dimension Icon, Bruker, USA) with silicon AFM tips (ScanAsyst-Air, Bruker, USA). Peak force tapping mode was used with a peak force tapping setpoint of 0.5 nN and a feedback gain of 10. The typical scan size was 10 μm × 10 μm and the scan rate was 1 Hz.

## 3. Results and Discussion

### 3.1. LEIS analysis of the topmost layer of pristine ISG surfaces

LEIS is well known for the sensitivity of the topmost atomic layer with very little interference from subsurface species.(27, 28) The fractured surface that has never been touched with any physical objects or chemicals could be assumed to be the most pristine surface that one can prepare. Even in that case, the surface composition may not be assumed to be the same as the bulk composition.(24) Relaxation and migration of surface atoms could alter the composition of surface different from that of the bulk even without any physical or chemical contacts.(26) The LEIS spectrum of the vacuum-fractured ISG surface is shown in Figure 1a. Note that B (10.8 amu) cannot be detected in this experimental condition. Also, Al (27 amu) versus Si (28 amu) as well as K (39 amu) versus Ca (40 amu) cannot be distinguished because their atomic masses are too close to each other. It is known that the LEIS sensitivity increases in proportion to atomic number.(28) Even if the mass difference is taken into account, the LEIS signal intensity of Na (23 amu) is found to be extremely high compared to that of Si. Figure 1b shows the normalized bulk and surface Na contents. The Na bulk content is obtained by normalizing the mole % of Na to that of O (Table 1). The Na content (normalized with oxygen peak) at the topmost atomic layer is about 5 times higher than what is expected from the bulk composition (Figure 1b). This result is consistent with the recent computational work predicting the Na enrichment at the glass / vacuum interface.(24)

Possible reasons for the surface enrichment of alkali ions on clean fractured surfaces were discussed in the literature. One factor contributing to this surface enrichment is the mechanical relaxation induced diffusion of alkalis toward the outermost surface.(26) The other factor might be the enhanced mobile cation diffusion due to the temperature rise at the tip of the moving crack during the fracturing process.(26) It is also possible that the negative charge at the fracture surface is the driving force for the migration of alkali cations to the surface.(30) During the fracturing process, the glass could also break along the percolation channel of Na ion clusters resulting in a surface enrichment of Na.(31, 32)

Surface enrichment of Ca on ISG surface upon fracturing in vacuum was also examined. The result show that, like Na, there is also a surface enrichment of Ca on vacuum-fractured ISG sample (see Supporting Information). The Ca concentration on the vacuum-fractured surface is 1.7 times higher than that in the bulk. This enrichment of Ca is opposite to what observed on trisilicate glass by Kelso et al.(26)

The LEIS spectra of ISG surface prepared by air-fracture and then immersion in ultra-pure water or silica-saturated aqueous solution for 100 s are also shown in Figure 1a. The normalized Na content at the topmost atomic layer is given in Figure 1b. The data shows that even after only 100 s in contact with aqueous solution, the Na content at the topmost atomic layer drops by 60 – 70% from the concentration of the pristine surface. It is interesting to note that the decrease of the Na signal is accompanied by the increase of the Si/Al signal. This could mean that the Na ions are masking the Si and Al network former sites at the topmost atomic layer of the vacuum-fractured surface. The Na content on the ISG sample immersed for 100 s in saturated silica solution (also containing $K^+$) is lower than that on the sample immersed in ultrapure water for 100 s. It could be due to the masking effect caused by $K^+$ and silicon containing species adsorbed from the silica

solution onto the ISG surface. Compared to the pristine surface, the Ca signal intensity is decreased after 100 s contact with ultrapure water. This implies that the leaching rate of Ca ions from the surface is faster than the replenishing rate through the diffusion from the bulk at this very early stage of corrosion. In the case of the silica-saturated solution treatment, the large increase in the K/Ca signal intensity is believed to be caused by the adsorption of $K^+$ ions from the solution phase. Overall, the results clearly show that even simple rinsing with water for a short period of time would alter the surface composition of ISG.

**3.2. Surface composition of aqueous-corroded ISG from LEIS and XPS**

Figure 2a shows LEIS spectra of air-fractured ISG samples corroded in silica-saturated solutions for different corrosion times. It was observed from these LEIS spectra that the background of the lower energy side of the Zr peak gets higher with corrosion time in aqueous solution. This low-energy tail could be attributed to backscattering in deeper porous alteration layer and its intensity is mainly determined by the reionization process.(4, 28) Thus, the results indicate that the alteration layer is porous, and $^4He^+$ ions can penetrate into the subsurface region, be neutralized, collide and scatter back to the outermost surface where they are re-ionized and then detected by the LEIS detector at energies lower than that of the main peak.(27, 28)

The area of Zr peak obtained from fittings was normalized to the area of O peak and given in Figure 2b. The normalized Zr contents of bulk ISG, ISG vacuum-fractured surface, and ISG air-fractured then immersed in ultra-pure water or silica saturated solutions for 100 sec (data from Figure 1a) are also shown for comparisons. The lower Zr content on the ISG sample immersed for 100 s in saturated silica solution in comparison to that on the sample immersed in ultrapure water for 100 s could, as in the case of Na content, be due to the masking effect caused by $K^+$ and silicon containing species adsorbed from the silica solution onto the ISG surface. The Zr surface contents

calculated from LEIS spectra of vacuum fractured ISG and ISG air-fractured then immersed in water or silica saturated solution are lower than the value calculated from the bulk composition. This difference could be explained by the masking effect of Na (in the case of vacuum fracture), $K^+$ and silicon containing species adsorbed from the silica solution onto the ISG surfaces. In Figure 2b, it can be seen that there is a significant enrichment of Zr on the ISG surface after being corroded in aqueous solutions for more than 1 hour.

A similar enrichment of Zr on corroded glass surfaces has been reported by Hellman and others.(33-37) In their studies, however, glass samples were corroded in dilute conditions of soluble silicon containing species. In these conditions and due to the extremely low solubility of zirconium oxide in comparison to others, it is reasonable to observe a surface enrichment of Zr on corroded glass samples. The corrosion behavior of glass has been shown to vary with zirconium and hafnium contents in the glass.(38-41) The study by Gin et al. showed a large enrichment of $^{29}Si$ on the outermost alteration layer formed on ISG corroded in aqueous solution initially saturated with amorphous $^{29}SiO_2$ at 90 $^oC$.(21) This study also showed that 2.3% of initial silicon atoms in the glass surface were replaced by $^{29}Si$ atoms present in the leaching solution. It means that there were a dissolution of surface network and condensation reactions between silicon containing species in the solution ($^{29}Si$) and Si species of the silicate network. It is again confirmed that surface dissolution still occurs in the initially silica-saturated solution.

The results obtained from LEIS experiments show a complete depletion of Na and a significant enrichment of Zr on the topmost surfaces of ISG corroded in aqueous solutions initially saturated with soluble silica. XPS analyses of the same corroded ISG samples were carried out to obtain the atomic concentrations of elements of the corroded surface averaged over the top 10 nm region. The results obtained are given in Figure 3. The atomic concentrations of detected elements

are shown as atomic %. Figure 3 shows that boron was completely depleted from the leached layers. The ISG sample corroded for 1 hour shows a small amount of sodium on its surface while samples corroded for longer times (1, 7 days) show negligible sodium concentrations. The increase of relative atomic percentage of Al and Si contents after 1-hour corrosion can be explained by dissolution of Na, B, and Ca from ISG into the solution phase. However, the Al and Si contents then decrease with longer corrosion time in aqueous solutions, which is accompanied with an increase of surface Zr content. These results suggest that surface dissolution of Al and Si is surely occurring, which leads to an enrichment of Zr that has extremely low solubility of its oxide in water. Both LEIS and XPS analysis results confirm the surface enrichment of Zr upon corrosion of ISG in silica-saturated solutions. The decrease of Na, B, Al, and Si contents also leads to an enrichment of Ca on ISG corroded for 1 day in aqueous solutions.

XPS was further used in this study to obtain depth profiles for Na, Zr, B, Al, and Ca elements for the air-fractured ISG surfaces corroded in silica saturated solutions. The elemental concentrations (at.%) of these elements are given in Figure 4. B and Na are completely depleted in the alteration layers. An enrichment of Zr on the outside surface is also observed, especially on ISG corroded for 7 days. Ca is present in the alteration with a significant concentration. It was reported to remain in the alteration layer of ISG corroded in silica saturated solutions, especially in solution without added electrolytes.(10) The XPS depth profiling results show that enrichment of Zr is only present on the outer surface of corroded ISG samples.

### 3.3. Surface topography changes of aqueous-corroded ISG

The glass surface corroded in the initially silica-saturated solutions has been studied assuming that Si, Al, and Zr do not dissolve from glass network into aqueous solution. While corrosion solutions were initially saturated with soluble silica, it does not warrant that there is a

true equilibrium between the $Q_n$ species (where n represents the number of bridging bonds) in the glass network and the silicic acid in aqueous solution. Due to this non-equilibrium nature, dissolution of Si and Al from glass surface is possible. As a result, the surface topography can change during the corrosion process. Figure 5 shows the topographic evolution of the ISG air-fractured surface before and after corrosion in silica saturated solution for different time. These AFM images reveal a significant change of surface topography due to the corrosion. The root means squares (RMS) of surface roughness are given in Figure 5f. The surface roughness of ISG sample increases significantly with corrosion time in aqueous solution. A change of surface topography of polished ISG samples corroded in pH 7 silica-saturated solutions at 90 $^{o}$C was reported by Liu et al.(11) The increase of RMS values with corrosion time is consistent with the stochastic dissolution phenomenon occurring at a flat surface.(42-45)

AFM was used by Mellott and others to study the change of surface roughness of fire polished glass and fiber surfaces after corrosion in aqueous solutions.(46) It was reported that there was no detectable roughening generated by cation leaching alone and the increase of surface roughness was due to network dissolution. The change of surface roughness was also correlated with the amount of silica dissolved into the solution.

### 3.4. Implication to Aqueous Corrosion Process

The results from spectroscopic analyses (LEIS and XPS) and topographic analysis (AFM) confirm that ISG is still dissolving even in the initially silica-saturated solution. The silicon containing species and their concentrations in aqueous solutions have been shown to vary with electrolyte concentrations.(47, 48) Using fast atom bombardment mass spectrometry, Tanaka and Takashima reported various silicon containing species in aqueous sodium chloride solutions and their total concentration increased with the NaCl concentration.(48) This finding suggests that the

leaching of Na and B from the ISG glass could alter the silica species present in the solution phase, which will be inevitably accompanied by the alteration of the saturation concentration of soluble silica species in the solution. This may lead to dissolution of silicate network formers from the glass.(49) The reverse process (precipitation of silica species onto the glass surface) is also possible if the silica saturation concentration is decreased because of leaching of modifier ions from the glass; if this happened in the case of ISG studied in this work, then the Zr surface concentration would have decreased in LEIS and XPS analyses.

The evidence of surface dissolution of glass samples even in the initially silica-saturated solutions may imply that there might be no true equilibrium between silicon-containing soluble species prepared with reference samples different from the glass composition and the silicate species in the network of the glass sample of interest at the beginning of the corrosion process. This study performed corrosion experiments for a short time (up to 7 days); however, it is important to keep in mind that the network dissolution observed in the beginning of the corrosion process is unlikely to occur in the alteration layer formed over a long exposure time; but, the behaviors at the initial stage may influence the subsequently-formed structure of the alteration layer because of the path-/history-dependence of non-equilibrium chemical reactions. The glass corrosion mechanism can change with time and it was observed for UK Magnox-waste glass that it took more than 28 days for its corrosion process at 90 $^{o}$C in deionized water to change from fully controlled ion exchange at the beginning to fully controlled hydrolysis.(50)

## 4. Conclusions

Surface dissolution of glass network in the initially silica-saturated solutions has been studied using surface-sensitive characterization techniques such as LEIS, XPS and AFM. Although

the thermodynamic affinity model predicts no loss of silicate network component because the soluble silica concentration was initially equilibrated with amorphous silica solid, the surface analysis results reveal evidence suggesting the dissolution of silicate network components from the glass surface. Mobile elements (B, Na) leached out from the glass might affect the saturation level of silicon-containing species in the aqueous phase and further studies on this effect are required to better understand glass corrosion.

**Supplementary Information**

Ca content calculated from the LEIS spectrum of vacuum-fractured ISG sample. The Supporting Information is available free of charge on the ACS Publications website at DOI:

**Acknowledgements.** This work was supported as part of the Center for Performance and Design of Nuclear Waste Forms and Containers, an Energy Frontier Research Center funded by the U.S. Department of Energy, Office of Science, Basic Energy Sciences under Award # DE-SC0016584. The authors thank Dr. Henry Luftman (Lehigh University) for LEIS measurements of ISG samples.

**References**

1. Collin M, Fournier M, Frugier P, Charpentier T, Moskura M, Deng L, et al. Structure of International Simple Glass and properties of passivating layer formed in circumneutral pH conditions. npj Materials Degradation. 2018;2(1):4.
2. Gin S, Guittonneau C, Godon N, Neff D, Rebiscoul D, Cabié M, et al. Nuclear Glass Durability: New Insight into Alteration Layer Properties. The Journal of Physical Chemistry C. 2011;115(38):18696-706.
3. Gin S, Abdelouas A, Criscenti LJ, Ebert WL, Ferrand K, Geisler T, et al. An international initiative on long-term behavior of high-level nuclear waste glass. Materials Today. 2013;16(6):243-8.

4. Ngo D, Liu H, Sheth N, Lopez-Hallman R, Podraza NJ, Collin M, et al. Spectroscopic ellipsometry study of thickness and porosity of the alteration layer formed on international simple glass surface in aqueous corrosion conditions. npj Materials Degradation. 2018;2(1):20.
5. Vienna JD, Ryan JV, Gin S, Inagaki Y. Current Understanding and Remaining Challenges in Modeling Long-Term Degradation of Borosilicate Nuclear Waste Glasses. International Journal of Applied Glass Science. 2013;4(4):283-94.
6. Vienna JD, Neeway JJ, Ryan JV, Kerisit SN. Impacts of glass composition, pH, and temperature on glass forward dissolution rate. npj Materials Degradation. 2018;2(1):22.
7. Frugier P, Gin S, Minet Y, Chave T, Bonin B, Godon N, et al. SON68 nuclear glass dissolution kinetics: Current state of knowledge and basis of the new GRAAL model. Journal of Nuclear Materials. 2008;380(1):8-21.
8. Fournier M, Gin S, Frugier P. Resumption of nuclear glass alteration: State of the art. Journal of Nuclear Materials. 2014;448(1):348-63.
9. Gin S, Collin M, Jollivet P, Fournier M, Minet Y, Dupuy L, et al. Dynamics of self-reorganization explains passivation of silicate glasses. Nature Communications. 2018;9(1):2169.
10. Collin M, Fournier M, Charpentier T, Moskura M, Gin S. Impact of alkali on the passivation of silicate glass. npj Materials Degradation. 2018;2(1):16.
11. Liu H, Ngo D, Ren M, Du J, Kim SH. Effects of surface initial condition on aqueous corrosion of glass—A study with a model nuclear waste glass. Journal of the American Ceramic Society. 2019;102(4):1652-64.
12. Gin S, Beaudoux X, Angéli F, Jégou C, Godon N. Effect of composition on the short-term and long-term dissolution rates of ten borosilicate glasses of increasing complexity from 3 to 30 oxides. Journal of Non-Crystalline Solids. 2012;358(18):2559-70.
13. Neill L, Gin S, Ducasse T, De Echave T, Fournier M, Jollivet P, et al. Various effects of magnetite on international simple glass (ISG) dissolution: implications for the long-term durability of nuclear glasses. npj Materials Degradation. 2017;1(1):1.
14. Jollivet P, Gin S, Schumacher S. Forward dissolution rate of silicate glasses of nuclear interest in clay-equilibrated groundwater. Chemical Geology. 2012;330-331:207-17.
15. Mcvay GL, Buckwalter CQ. Effect of Iron on Waste-Glass Leaching. Journal of the American Ceramic Society. 1983;66(3):170-4.
16. Dove PM, Nix CJ. The influence of the alkaline earth cations, magnesium, calcium, and barium on the dissolution kinetics of quartz. Geochimica et Cosmochimica Acta. 1997;61(16):3329-40.
17. Aagaard P, Helgeson HC. Thermodynamic and kinetic constraints on reaction rates among minerals and aqueous solutions; I, Theoretical considerations. American journal of Science. 1982;282(3):237-85.
18. Grambow B, Müller R. First-order dissolution rate law and the role of surface layers in glass performance assessment. Journal of Nuclear Materials. 2001;298(1):112-24.
19. Gin S, Frugier P, Jollivet P, Bruguier F, Curti E. New Insight into the Residual Rate of Borosilicate Glasses: Effect of S/V and Glass Composition. International Journal of Applied Glass Science. 2013;4(4):371-82.
20. Gin S, Jollivet P, Fournier M, Angeli F, Frugier P, Charpentier T. Origin and consequences of silicate glass passivation by surface layers. Nature Communications. 2015;6:6360.
21. Gin S, Jollivet P, Barba Rossa G, Tribet M, Mougnaud S, Collin M, et al. Atom-Probe Tomography, TEM and ToF-SIMS study of borosilicate glass alteration rim: A multiscale

approach to investigating rate-limiting mechanisms. Geochimica et Cosmochimica Acta. 2017;202(Supplement C):57-76.
22. Kobayashi T, Sasaki T, Takagi I, Moriyama H. Solubility of zirconium (IV) hydrous oxides. Journal of Nuclear Science and technology. 2007;44(1):90-4.
23. Gin S, Jollivet P, Fournier M, Berthon C, Wang Z, Mitroshkov A, et al. The fate of silicon during glass corrosion under alkaline conditions: A mechanistic and kinetic study with the International Simple Glass. Geochimica et Cosmochimica Acta. 2015;151:68-85.
24. Ren M, Deng L, Du J. Bulk, surface structures and properties of sodium borosilicate and boroaluminosilicate nuclear waste glasses from molecular dynamics simulations. Journal of Non-Crystalline Solids. 2017;476:87-94.
25. Morey GW, Fournier RO, Rowe JJ. The solubility of amorphous silica at 25°C. Journal of Geophysical Research (1896-1977). 1964;69(10):1995-2002.
26. Almeida RM, Jain H, Pantano CG. Low-Energy Ion-Scattering Spectroscopy of Modified Silicate Glasses. Journal of the American Ceramic Society. 2016;99(4):1259-65.
27. Cushman CV, Brüner P, Zakel J, Major GH, Lunt BM, Smith NJ, et al. Low energy ion scattering (LEIS). A practical introduction to its theory, instrumentation, and applications. Analytical Methods. 2016;8(17):3419-39.
28. Brongersma HH, Draxler M, de Ridder M, Bauer P. Surface composition analysis by low-energy ion scattering. Surface Science Reports. 2007;62(3):63-109.
29. Liu H, Ngo D, Ren M, Du J, Kim SH. Effects of surface initial condition on aqueous corrosion of glass—A study with a model nuclear waste glass. Journal of the American Ceramic Society.0(0).
30. Kelso JF, Pantano CG, Garofalini SH. A comparison of ion scattering spectra and molecular dynamics simulations at the surface of silicate glasses. Surface Science. 1983;134(3):L543-L9.
31. Ojovan MI. Mass spectrometric evidencing on modified random network microstructure and medium range order in silicate glasses. Journal of Non-Crystalline Solids. 2016;434:71-8.
32. Greaves GN. EXAFS and the structure of glass. Journal of Non-Crystalline Solids. 1985;71(1):203-17.
33. Abdelouas A, Crovisier J-L, Lutze W, Mueller R, Bernotat W. Structure and chemical properties of surface layers developed on R7T7 simulated nuclear waste glass altered in brine at 190 degrees C. European Journal of Mineralogy. 1995;7(5):1101-13.
34. Hellmann R, Cotte S, Cadel E, Malladi S, Karlsson LS, Lozano-Perez S, et al. Nanometre-scale evidence for interfacial dissolution–reprecipitation control of silicate glass corrosion. Nature Materials. 2015;14:307.
35. Valle N, Verney-Carron A, Sterpenich J, Libourel G, Deloule E, Jollivet P. Elemental and isotopic (29Si and 18O) tracing of glass alteration mechanisms. Geochimica et Cosmochimica Acta. 2010;74(12):3412-31.
36. Lenting C, Plümper O, Kilburn M, Guagliardo P, Klinkenberg M, Geisler T. Towards a unifying mechanistic model for silicate glass corrosion. npj Materials Degradation. 2018;2(1):28.
37. Hopf J, Eskelsen JR, Chiu M, Ievlev AV, Ovchinnikova OS, Leonard D, et al. Toward an understanding of surface layer formation, growth, and transformation at the glass–fluid interface. Geochimica et Cosmochimica Acta. 2018;229:65-84.
38. Hopf J, Kerisit SN, Angeli F, Charpentier T, Icenhower JP, McGrail BP, et al. Glass–water interaction: Effect of high-valence cations on glass structure and chemical durability. Geochimica et Cosmochimica Acta. 2016;181:54-71.

39. Cailleteau C, Angeli F, Devreux F, Gin S, Jestin J, Jollivet P, et al. Insight into silicate-glass corrosion mechanisms. Nature Materials. 2008;7:978.
40. Bergeron B, Galoisy L, Jollivet P, Angeli F, Charpentier T, Calas G, et al. First investigations of the influence of IVB elements (Ti, Zr, and Hf) on the chemical durability of soda-lime borosilicate glasses. Journal of Non-Crystalline Solids. 2010;356(44):2315-22.
41. Cailleteau C, Devreux Fo, Spalla O, Angeli F, Gin S. Why do certain glasses with a high dissolution rate undergo a low degree of corrosion? The Journal of Physical Chemistry C. 2011;115(13):5846-55.
42. Bandstra JZ, Brantley SL. Surface evolution of dissolving minerals investigated with a kinetic Ising model. Geochimica et Cosmochimica Acta. 2008;72(11):2587-600.
43. Hernández-Creus A, Carro P, Salvarezza R, Arvia A. A Monte Carlo simulation of roughness development during the dissolution of a pure solid. Journal of The Electrochemical Society. 1995;142(11):3806-11.
44. Mack CA. Stochastic modeling in lithography: the use of dynamical scaling in photoresist development: SPIE; 2009.
45. Hopf J, Pierce EM. Topography and Mechanical Property Mapping of International Simple Glass Surfaces with Atomic Force Microscopy. Procedia Materials Science. 2014;7:216-22.
46. Mellott NP, Pantano CG. A Mechanism of Corrosion-Induced Roughening of Glass Surfaces. International Journal of Applied Glass Science. 2013;4(3):274-9.
47. Harris RK, Newman RH. 29Si N.M.R. studies of aqueous silicate solutions. Journal of the Chemical Society, Faraday Transactions 2: Molecular and Chemical Physics. 1977;73(7):1204-15.
48. Tanaka M, Takahashi K. Characterization of Silicate Complexes in Aqueous Sodium Sulfate Solutions by FAB-MS. Journal of Solution Chemistry. 2005;34(6):617-30.
49. Schaefer J, Backus EHG, Bonn M. Evidence for auto-catalytic mineral dissolution from surface-specific vibrational spectroscopy. Nature Communications. 2018;9(1):3316.
50. Ojovan MI, Pankov A, Lee WE. The ion exchange phase in corrosion of nuclear waste glasses. Journal of Nuclear Materials. 2006;358(1):57-68.

**List of Table Captions**

**Table 1.** Elemental molar composition of ISG (based on wt% of ingredients provided by MO-SCI, Corp).

**List of Figure Captions**

**Figure 1.** (a) LEIS spectra of the pristine (vacuum-fractured) ISG surface and the surface contacted with aqueous solutions (ultra-pure water and silica-saturated water) for 100 seconds after air fracture. (b) Na content calculated from the LEIS spectra. The normalized bulk concentration of Na (from Table 1) is also shown for comparison.

**Figure 2.** ISG fractured in air and corroded in 90 $^{o}$C, pH7, silica saturated solution (with $K^{+}$ ions): (a) LEIS spectra; (b) normalized Zr content.

**Figure 3.** Elemental concentration (atomic %) for Na, B, Ca, Al, Si, and Zr determined from XPS analysis of the fractured ISG (bulk) and the surfaces corroded for varying times (from 1 hour up to 7 days) in pH 7 aqueous solution initially saturated with soluble silica species at 90 $^{o}$C.

**Figure 4**. XPS depth profiles of air-fractured ISG glass corroded in pH7 silica-saturated solutions at 90 $^{o}$C: (a) 1 hour, (b) 1 day, (c) 7 days.

**Figure 5.** AFM images of ISG fractured samples corroded in 90 $^{o}$C, pH7, silica saturated (with $K^{+}$ ions) solution for (a) 0 hour (uncorroded); (b) 1 hour; (c) 1 day; (d) 7 days. Figure (e) shows RMS values of surface roughness.

## Tables

**Table 1.** Elemental molar composition of ISG (based on wt% of ingredients provided by MO-SCI, Corp).

| Element | Si | B | Na | Al | Ca | Z | O |
|---|---|---|---|---|---|---|---|
| **Mol%** | 17.99 | 9.73 | 7.68 | 2.22 | 1.56 | 0.50 | 60.31 |

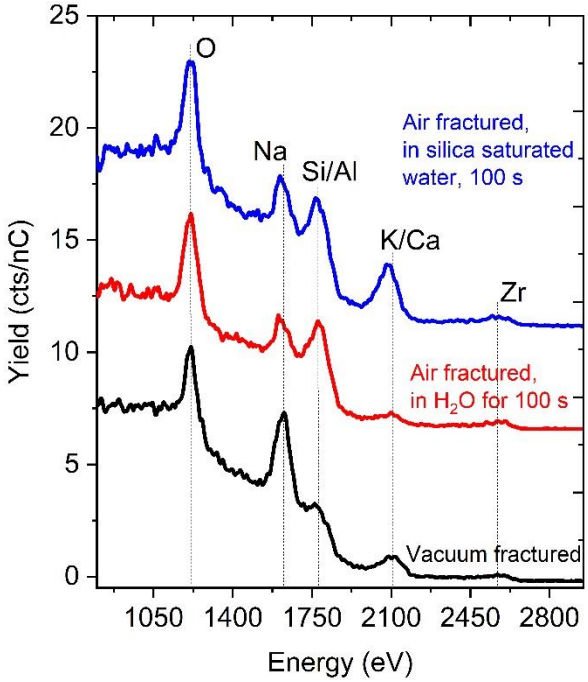
O
Na
Si/Al
K/Ca
Zr
Air fractured,
in silica saturated
water, 100 s
Air fractured,
in $H_2O$ for 100 s
Vacuum fractured
Yield (cts/nC)
Energy (eV)
25
20
15
10
5
0
1050
1400
1750
2100
2450
2800

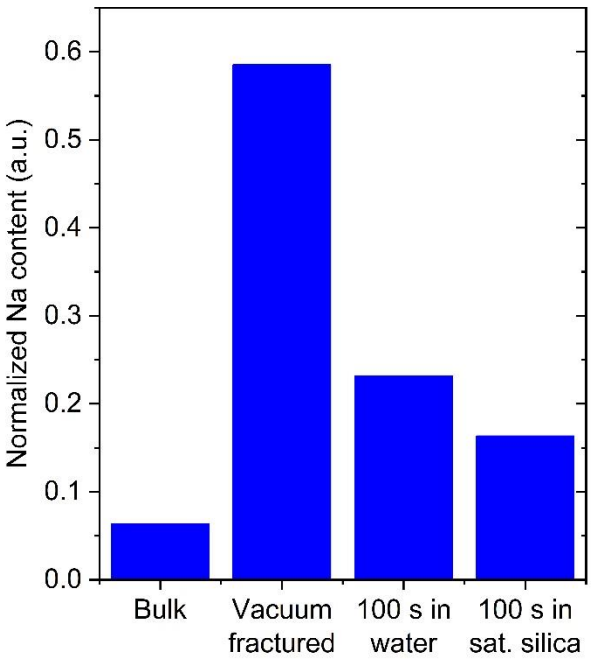
Normalized Na content (a.u.)
0.6
0.5
0.4
0.3
0.2
0.1
0.0
Bulk
Vacuum fractured
100 s in water
100 s in sat. silica

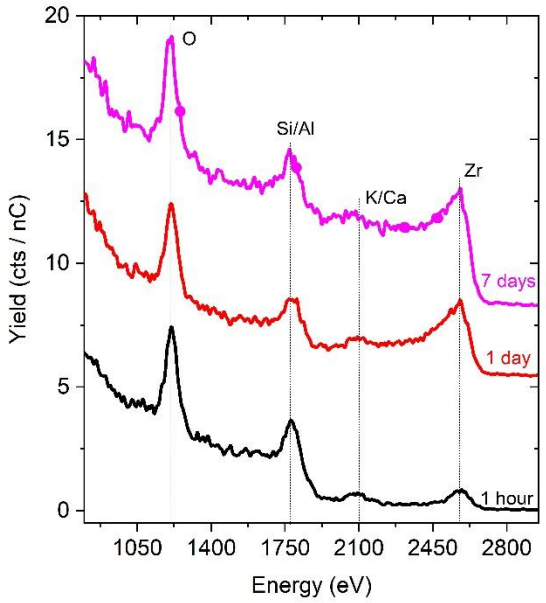
Yield (cts / nC)
Energy (eV)
O
Si/Al
K/Ca
Zr
7 days
1 day
1 hour

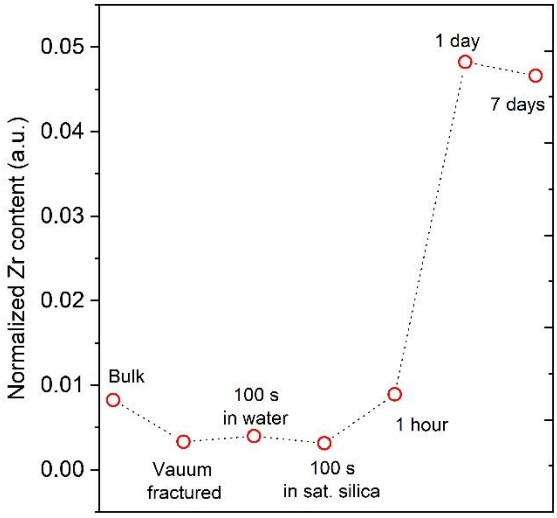
Normalized Zr content (a.u.)
Bulk
Vauum fractured
100 s in water
100 s in sat. silica
1 hour
1 day
7 days

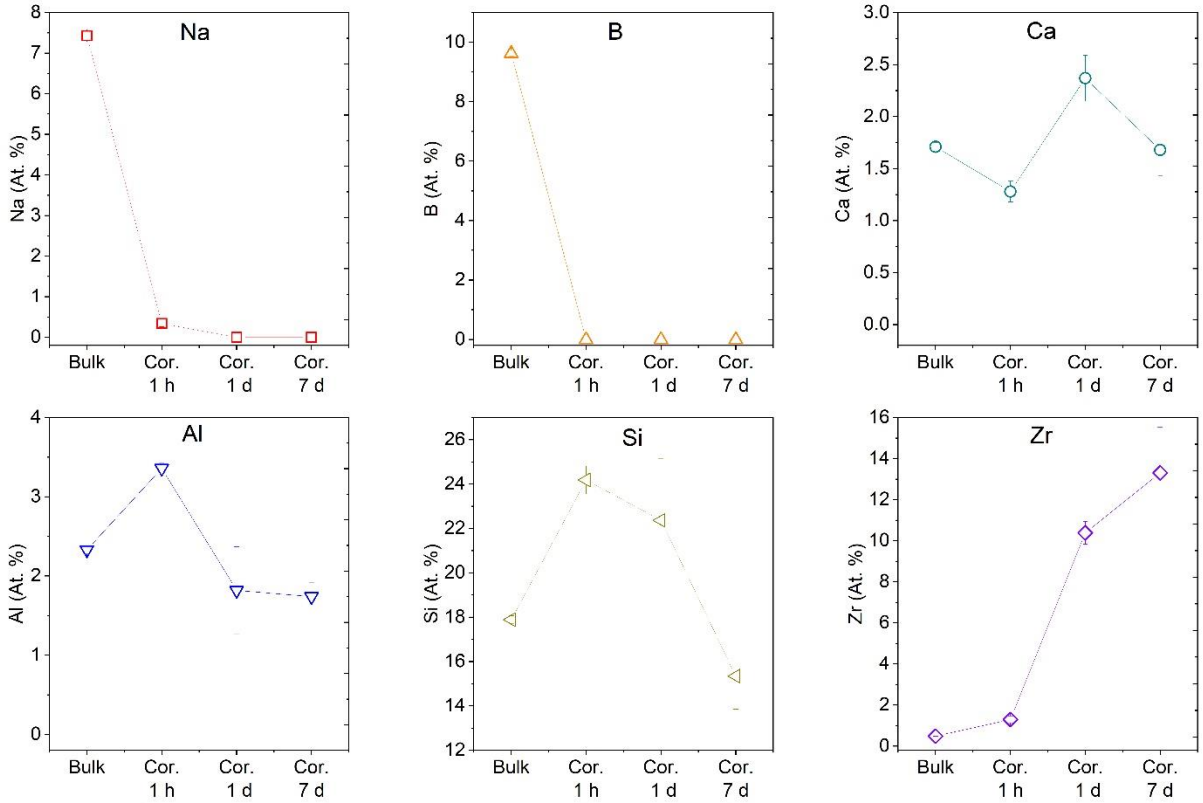
Na
Na (At. %)
B
B (At. %)
Ca
Ca (At. %)
Al
Al (At. %)
Si
Si (At. %)
Zr
Zr (At. %)
Bulk
Cor. 1 h
Cor. 1 d
Cor. 7 d

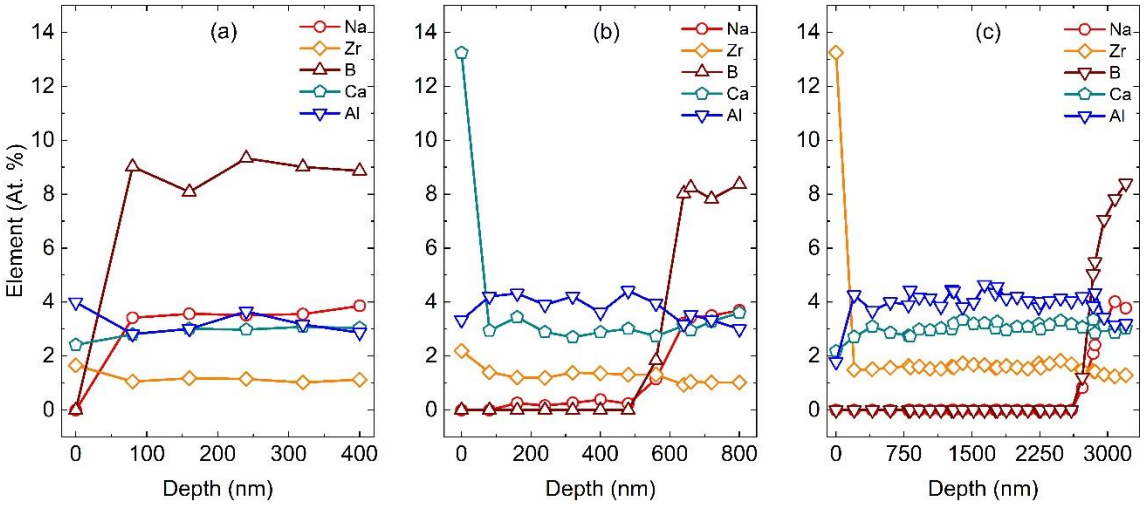
(a)
(b)
(c)
Na
Zr
B
Ca
Al
Element (At. %)
Depth (nm)
0
2
4
6
8
10
12
14
0
100
200
300
400
600
800
750
1500
2250
3000

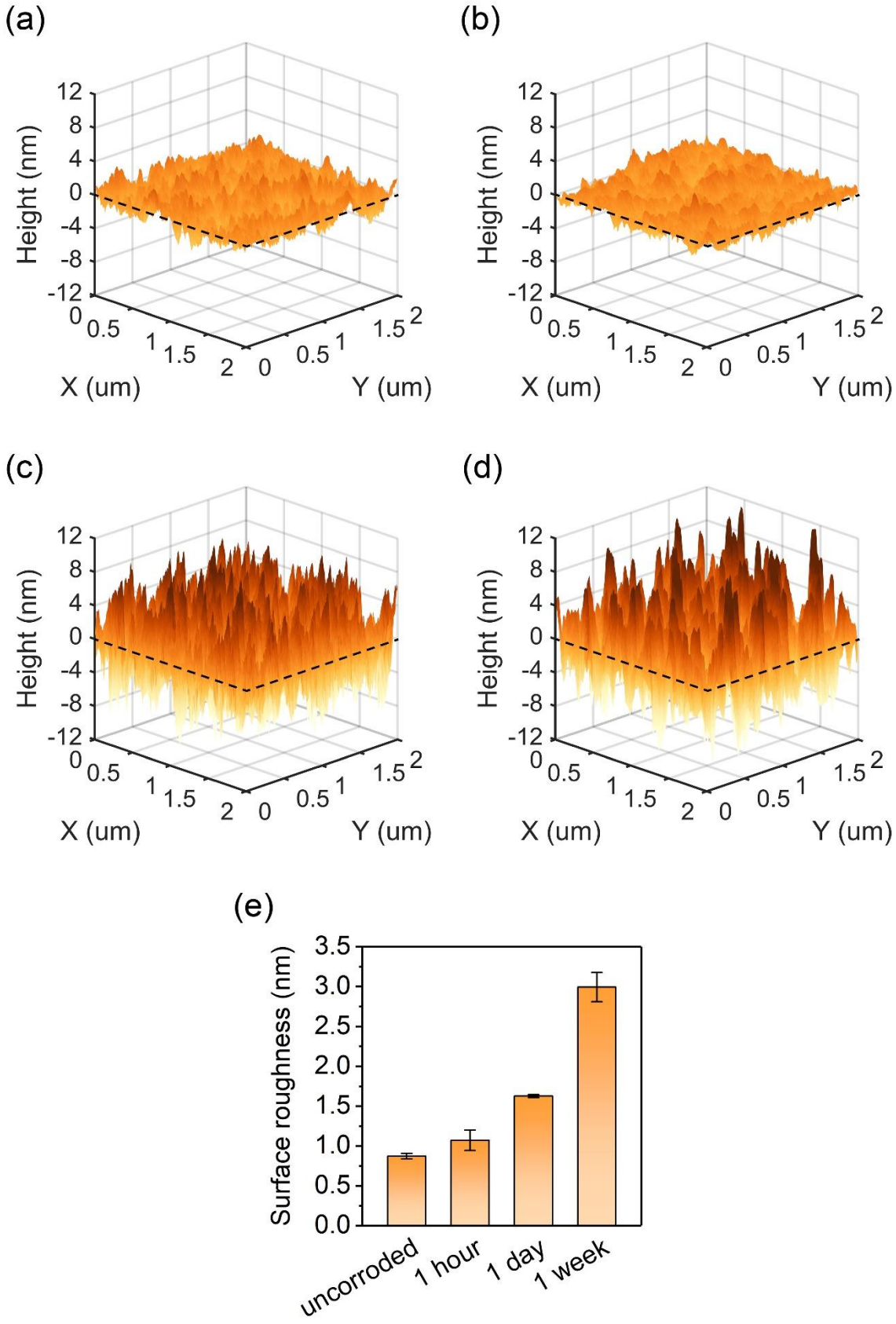
(a)
(b)
(c)
(d)
(e)
Height (nm)
X (um)
Y (um)
Surface roughness (nm)
uncorroded
1 hour
1 day
1 week